Metals and Materials International (2019) 25:1457–1466
https://doi.org/10.1007/s12540-019-00300-8

Effect of Ni Addition on the Morphology and Microstructure of Both Conventional Cast and Melt-Spun of Al–Si–Fe–Nb (at wt%) Alloy

M. Fatih Kilicaslan[1] · Salaheddin Salem Altaib[2] · Can Doğan Vurdu[3]

Received: 11 February 2019 / Accepted: 14 May 2019 / Published online: 22 May 2019

Abstract
In this project the morphology and microstructure of both conventional cast and melt spun of Al–20Si–9Fe–1.2Nb and Al–20Si–9Fe–1.2Nb–6Ni (at wt%) alloys were investigated. Therefore, in order to study the effect of added Ni on the morphology characteristics of the above-mentioned alloy, the resulting conventional cast and ribbons of Al–20Si–9Fe–1.2Nb and Al–20Si–9Fe–1.2Nb–6Ni alloys were synthesized and analysed using OM optical microscopy, X-ray diffraction, SEM scanning electron microscopy together with EDS energy dispersive spectroscopy. Observations exhibit that, XRD patterns of Al–Si–Fe–Nb and Al–Si–Fe–Nb–Ni ribbons revealed the peaks of only α-Al phase. Therefore, after adding of 6 wt% Ni, peaks of α-Al were shifted to the relatively lower angles with a very weak intensity. Furthermore, 6 wt% Ni addition causes homogeneously scattered colonies (size range 5 –25 μm) which contain fine spherical (primary Si and δ-Al_4(FeNiNb)Si_2 phases) particles in the α-Al dendrite of rapidly solidified Al–20Si–9Fe–1.2Nb alloy, the size of spherical particles were found to be in the range of 100 nm–1 μm.

Keywords Al–Si–Fe–Nb alloy · Melt-spun · XRD · Microstructure

1 Introduction

Nowadays, a great amount of research considers investigation of metallic glass materials with different composition, due to their unique disorder structure and mechanical properties, which makes them attractive candidate in a wide range of application [1, 2]. Although, aluminium, magnesium and their alloys are the commonly used within light materials in the manufacturing sectors for aeronautical and automotive parts. The great interest for light weight technology are Al-based amorphous materials according to their indispensable mechanical and physical features, due to its excellent corrosion resistance, ease of manufacturing, elevated strength to weight ratio and high electrical as well as thermal conductivity [3–6]. In practice, among the different rapid solidification processes, the melt-spinning process grants big advantages over its competing (industrial) techniques for its highest cooling rate (10^5 to 10^7 k/s), a condition that the viscosity increases, and the configuration entropy drastically decreases till the material reach the glass transition temperature, identified by a viscosity of about $\eta = 10^{13}$ poise. In addition to that, the best score in cost/performance ratio [7–11]. In 1981, the first amorphous single-phase Al-based alloys were formed, including Al–Fe–B and Al–Co–B ternary alloys [12]. According to the most published researches two classes of Al-based alloy have widely been produced using melt-spinning machines (1) crystalline Al-alloys that shows extremely low equilibrium solubility in Al-matrix (e.g, Zr, Ni, Mn, Fe, Ti, etc.) such as Al–Fe–Cr alloys, Al–Si–Zr alloy, Al–Mn–Fe alloy, Al–20Si–5Fe–2X (X = Ni or Cr) and Al–Fe–Cr alloy, etc. (2) Al-based amorphous alloys, including Al–R (R = rare earth metals, e.g,Y, La, Gd, Ce, Tb, Pr, Ho, Dy, Er, Sm), Al–EM–LM (EM, early transition metal including Zr, Nb, Cr, Mo, Ta, Ti, W or Hf. LM, late transition metal including Cu, Co, Fe or Ni) and Al–R–M (M = transition metal). Therefore, the ribbons of mentioned Al-alloy glasses were performed as precursors to prepare bulk

✉ M. Fatih Kilicaslan
fatihkilicaslan@yahoo.com; fkilicarslan@kastamonu.edu.tr

[1] Department of Mechanical Engineering, Faculty of Engineering and Architecture, Kastamonu University, Kastamonu, Turkey

[2] Department of Materials Science and Engineering, Institute of Science and Technology, Kastamonu University, Kastamonu, Turkey

[3] Department of Biomedical Engineering, Faculty of Engineering and Architecture, Kastamonu University, Kastamonu, Turkey

Al-based alloys with nanogranular structures for the Al-based ribbons while bulk Al-based alloys strengthened by quasicrystal line on nanoscale particles for crystalline Al-based alloys [8, 13–15]. Chain of strategies have been developed so as to stabilize the amorphous alloys in order to minimize the diffusion ability of the component atoms, that assumed to be precondition for the occurrence of crystallization [16]; (1) to limit long range diffusion of atoms, negative heat of mixing between component elements must be increased, e.g adding Pd to Al–Y–Ni based amorphous alloy, (2) obtaining low diffusion ability by introducing elements with a very large atomic size, e.g adding of La and Co to Al–Ni–Er ternary alloy. Even though, the elements with small atomic size have a drastic enhancement to a glass forming ability due to their large negative heat of mixing, e.g Oxygen added to Zr–Cu–Hf–Ti–Ni alloy, (3) increasing the viscosity of the alloy melt, in order to achieve higher thermal stability, e.g adding of Sc to Al–Y–Ni alloy [17–20], even in addition, Aronin [21] has stated that treatment of the amorphous phase within the amorphous state provides a nanocrystalline structure in case of Nano crystalline phase. Melt-spun Al–Si alloys have significant exception in automotive industry which exhibit excellent wear resistance, elevated temperature strength compared to the conventional alloys. Essentially, the most important modifiers for Al–Si alloy is Fe. Therefore, Fe-bearing intermetallic are harmful to mechanical properties related to its brittleness, modification of Si particles and Fe phases can be obtained by different fabrication techniques e.g melt-spinning process [5, 11, 22]. As a consequence, referring to the above discussion the target of this work is introducing 6 at wt% Ni to Al–20Si–9Fe–1.2Nb alloy, studying the microstructure and morphology of both as-cast and ribbons of mentioned alloys, in order to analyse and synthesise the effect of Ni addition .

2 Experimental

Alloys Al–Si–Fe–Nb and Al–Si–Fe–Nb–Ni with nominal compositions as given in Table 1 (at wt%), are prepared as follow, bulk ingots of suitable compositions are produced by Induction Furnace, the mixture of high purity elements (Al, 99.99%; Nb, 99.99%; Fe, 99.99%; Si, 99.99%; Ni, 99.99%) are prepared and melted in graphite crucible many times to ensure chemical homogeneity. Some additive materials melted prior to alloy melting to react with residual oxygen and nitrogen in the chamber. Ribbons were produced by using melt-spinning machine which is mainly consisting of graphite container for melting process and copper rotating disc for quenching (rapid solidify). The above mentioned compositions were melted and pressurized by means of argon through the 2 mm nozzle onto the rotating wheel under atmosphere condition. As the wheel moves (with a diameter 250 mm, and a circumferential speed 0f 20 m/s), the molten material is impinging on the cylindrical surface of polished brass wheel which is finally separated and spread a way in the form of a solidified strip (ribbons with dimensions of about 1–8 mm in width, and 20–30 µm thickness). Al–Si–Fe–Nb and Al–Si–Fe–Nb–Ni conventional casts are denoted as AlCC1 and AlCC2 respectively, while Al–Si–Fe–Nb and Al–Si–Fe–Nb–Ni melt-spun are denoted as AlMS1and AlMS2 respectively in this study. The microstructure of both ribbons and the conventional casts were graphically characterised by optical microscopy (OM, Leica), scanning electron microscopy (SEM) linked with EDS energy dispersive spectroscopy (SEM, FEI, Model: Quanta FEG 250), samples of mentioned compositions were embedded in epoxy resin then polished and etched in Keller's reagent (2 ml HF + 3 ml HCI + 5 ml HNO_3 + 190 ml H_2O, special for aluminium alloys) in order to perfectly flat and scratch samples free when viewed with the aid of a microscope devices. The phases and the microstructure of samples are characterized by X-ray diffraction (XRD) analysis was carried out by a (Bruker. model: D8 Advance) with Cu Kα radiation (λ = 1.5404 A˚) at 2θ-step of 0.15°, within a range of 25°–70°. Where the all mentioned work and tests was prepared in the laboratories of Kastamonu University.

Table 1 Chemical composition of Al alloys investigated (wt%)

	Al	Si	Fe	Nb	Ni
AlCC1 and AlMS1	69.8	20	9	1.2	–
AlCC2 and AlMS2	63.8	20	9	1.2	6

3 Results and Discussion

3.1 X-ray Diffraction

The phase constitution of quaternary alloys AlCC1 and AlMS1 were identified using XRD patterns are shown in Fig. 1a, b. It is evident that, α-Al has sharp crystalline peaks on the both pattern of the mentioned samples. From Fig. 1a samples of AlCC1 are fragmentary and fully crystalline, diffraction of peaks of Al and other (Fe-intermetallic) phases are clearly observed. One can notice that the most tow strongest and sharp peaks at 38.035° and 44.35° (2θ) are belonging to α-Al phase, while Si phase peaks are revealing in different (2θ) 28.2°, 47.1° and 55.9° with lower intensity counts. However, iron has very limited solubility in aluminium, all the iron was added to Al–Si to form intermetallic compounds δ-(Al_4FeSi_2) and β-(Al_5FeSi) phases, which presented by a weak and broad peaks diffraction patterns at 34.05°, 43.3°, 45.15° and 48.3° (2θ). In contrast, Fig. 1b shows that only some of α-Al peaks can be observed at 38.296°, 44.61° and 65.09° (2θ), while peaks of Si, δ (Al_4FeSi_2) and β-(Al_5FeSi) phases have totally been dispersed after melt-spinning process. Figure 3a, b showed

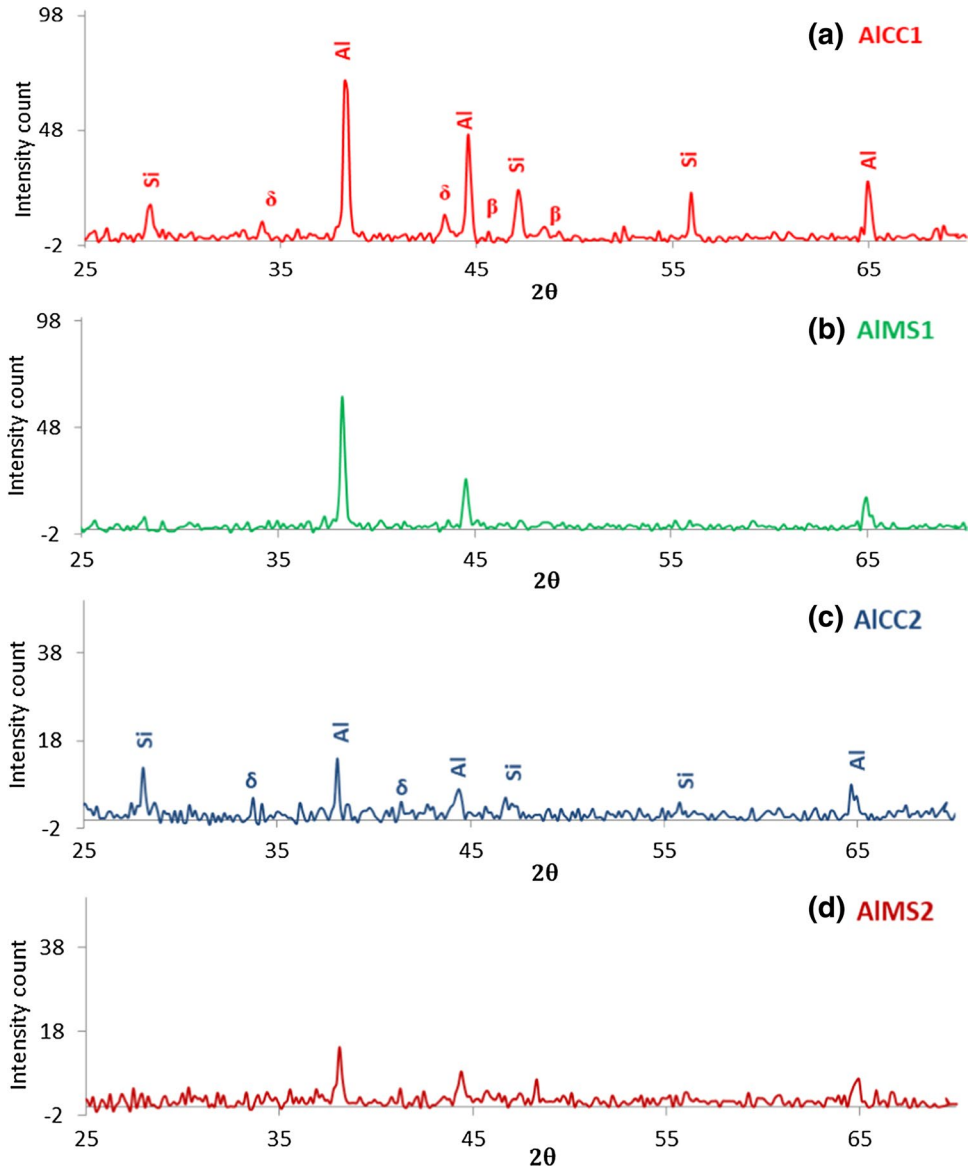

Fig. 1 The XRD diffraction patterns taken from: **a** AlCC1, **b** AlMS1, **c** AlCC2 and **d** AlMS2

Table 2 α-Al crystallographic data of samples at largest peaks

Sample	2θ (°)	Int. counts %	Lattice par. (nm)
AlCC1	38.035	64.5	0.4094
AlMS1	38.296	62.3	0.4067
AlCC2	38.217	13.97	0.4075
AlMS2	38.035	14.97	0.4094

how the structure refined after rapid solidified process, while crystallographic data obtained from XRD analysis of the α-Al peaks summarized in Table 2. The α-Al peaks of AlMS1 were found to be slightly shifted to little higher angles comparing with those of AlCC1as seen in Fig. 2, and the value of α-Al lattice parameter of AlMS1 is 0.4067 nm and for AlCC1 is (0.4094 nm), these values slightly larger than that of pure Al (0.4049 nm). Such changes of the diffraction angles and lattice values interpreted that some amount of either Nb or Fe was remained in solid solution in Al phase, in addition to the formation of supersaturated solid solution during RS process [1, 23]. One more reason for lattice enlargements it may related to atomic radii of compositions Al (0.143 pm) > Fe(0.132 pm) > Si (0.111 pm) but Nb (0.164 pm) is larger than that of Al that resulted in lattice increment [24] . Referred to XRD analysis of melt-spun Al–Si–Fe stated in [25] addition of Nb to Al–Si–Fe alloy has remarkable improvement on the diffraction pattern of AlMS1 Fig. 1b, but compared to Ünlü research [11] Nb addition to Al–Si–Fe alloy has no effect on the produced ribbons and this may related to the difference in chemical composition of used alloys.

Bragg equation for evaluating lattice parameters

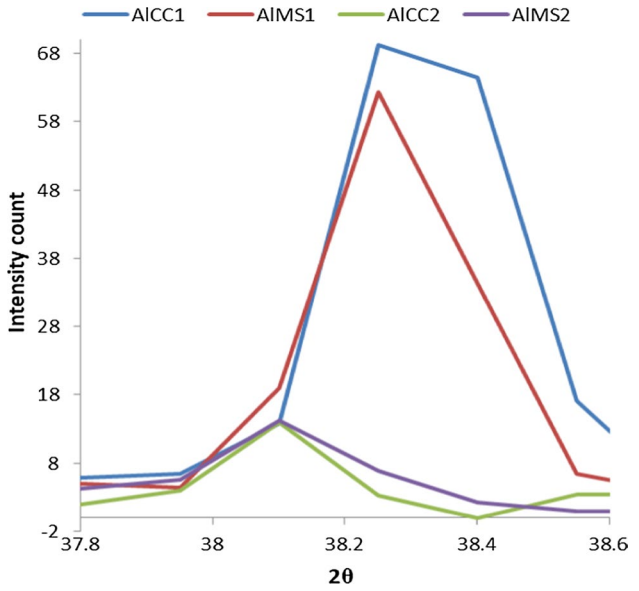

Fig. 2 XRD diffraction patterns of samples AlCC1, AlMS1, AlCC2 and AlMS2, illustrating the shifts of highest peaks intensity of (111) Al

$$n\lambda = 2d\sin(\theta) \quad (1)$$

$$a = d * (h^2 + k^2 + l^2)^{1}/_{2} \quad (2)$$

where λ = 0.15,404 nm, d-spacing, a-lattice parameter, {hkl}-Miller indices and θ-peak Bragg angle [26].

Figure 1c, d represent the XRD patterns of AlCC2 and AlMS2 samples respectively. In Fig. 1c the XRD patterns of AlCC2 presents Bragg peaks of the following phases α-Al, δ-Al(FeNiNb)Si and Si. It is clear that from Fig. 1c the revealed diffraction peaks were belonging to α-Al and Si phases, specifically Bragg Peak angles (38.03°, 44.25°, 64.65° and 77.7°) (2θ) represent α-Al phase, while Si peak at 28.05° (2θ). In contrast, intermetallic diffraction peak were (very low) almost completely disappeared.

Figure 1d represents XRD diffraction patterns of AlMS2 samples. It is obvious from Fig. 1d that the only diffraction peaks of α-Al are visible with relatively low intensity counts. In reference to diffraction patterns of AlCC2, α-Al diffraction peak of AlMS2 is slightly shifted to the lower Bragg peak angle from 38.21° to 38.03° (2θ) as illustrated in Fig. 2, while the lattice parameter was increased from 0.4075 to 0.4094 nm. The results have indicated over equilibrium of Si dissolution in aluminium lattice due to undercooling. In addition, the extended solid solubility of Ni during RS process, and Ni added to the main alloy, this has an agreement with [27] which reported that the solubility of Si in Al increases with increment of Ni quantity.

Furthermore, the absence of intermetallic phase at X-ray diffraction pattern denoted to extended solid solubility of Al matrix [28]. Figure 3c, d show the difference in surface shapes of both AlCC2 and AlMS2 respectively.

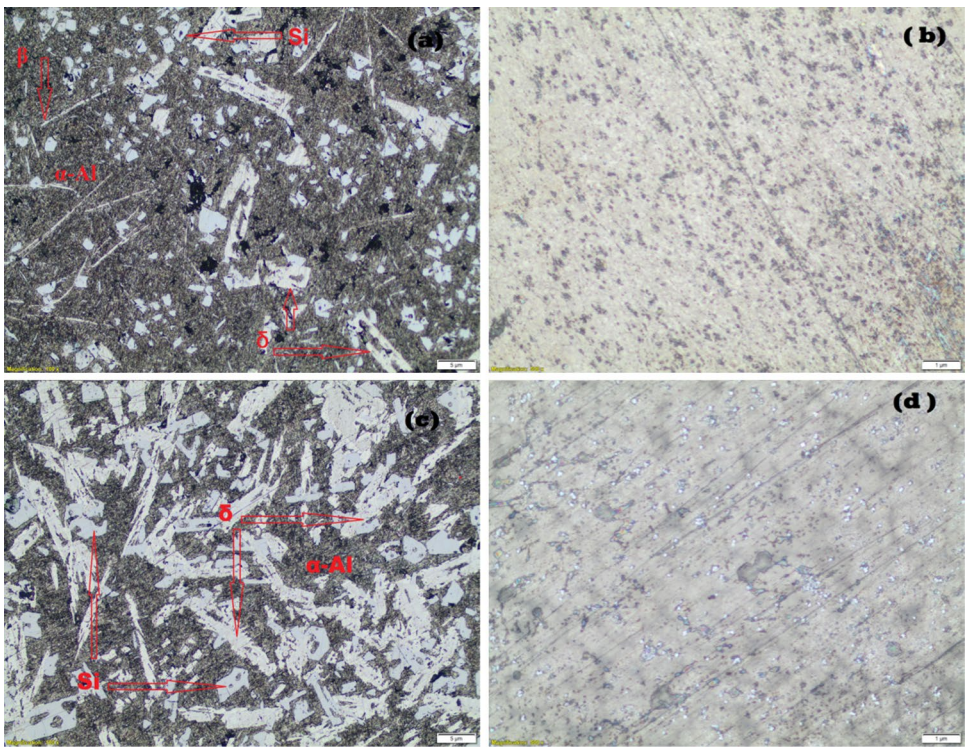

Fig. 3 Optical microscopy micrographs of: **a** AlCC1, **b** AlMS1, **c** AlCC2 and **d** AlMS2

3.2 Microstructure Change During Melt-Spinning

3.2.1 Microstructure of Conventional Cast AlCC1 and Melt-Spun AlMS1

The typical optical micrographs of AlCC1 and AlMS1 are illustrated by Fig. 3a, b respectively, it can be seen that the microstructure of AlCC1 in Fig. 3a it is mainly consisted of three phases: (1) intermetallic compound β-Al_5(FeNb)Si which presented as a white needle with different dimensions (0.2–1.5 µm × 2–10 µm) and latitudes, (2) small plate-lets of δ-Al_4(FeNb)Si_2 with dimension of about (2 µm × 4 µm), (3) Si phase exposed to be as a different relatively squared geometrical shapes of about (0.5–3 µm) size and the dark area that equipped the vast majority of the micrograph represents α-Al matrix, that even contains a tiny particles of (Nb, Si). Whereas, the melt-spun AlMS1 OM micrograph is illustrated in Fig. 3b, its microstructure is uniform and fine with dispersion of some crystals, it appears to be feature less after etching because to high quench rate that exposed to [11, 29]. In order to obtain a more microstructural characterization, the samples also investigated by SEM microscopy. Figure 4a, b, c show the SEM micrographs of conventional cast AlCC1 in different scales of magnification, Fig. 4a display the microstructure of phases as mentioned and explained in Fig. 3a, however, in Fig. 4b, c goes deeply to describe the morphology in scale of 0.5–5 µm, it is noticed that the phases revealed in shapes of sharp edged polygons with different dimensions ranged from 0.5 to 6 µm, it can be even seen that some spots of dimension (100 nm to 400 nm) Spread randomly over the polygons, which may be attributed to either Nb or Si particles.

EDS line scanning in Fig. 5a–c verified that Nb particles were dissolved homogeneously in base alloy which is confirmed that Nb and Fe is included into the mentioned intermetallic compounds in the Al matrix, while Si not completely dissolved and just spread on boundary of aluminium [30],which indicated an agreement with XRD analysis diffraction peaks of Si in Fig. 1a.

On the other hand, the melt-spun AlMS1 alloy was perceived as a very fine polygonal structure which is mainly composed of the α-Al phase (dark phase) and intermetallic δ-Al_4(FeNb)Si_2 phase (light grey phase) as illustrated in Fig. 6a, b, these cellular and dendrites are in size approximately between 2 µm to 5 µm, while dendrite arms average diameters approximately (200 nm–2 µm). Hence, the solid solubility of α-Al is extended because of rapid solidification process [30], all the compositions are dissolved and dispersed in α-Al matrix, which is confirmed by XRD diffraction pattern analysis in Fig. 1b through the absence of Si and δ-Al_4(FeNb)Si_2 diffraction peaks. Moreover, this resulted homogeneity of morphology suggested that the solidification in this region occurred in very similar manner. Figure 6c displays the morphology of precipitated particles of composition in α-Al in high magnification, which are agglomerated in aluminium matrix as dendritic rounded shapes. In other words, the interface between particles and amorphous matrix is misty, opposite to those pyramidal sharp polygons of conventional cast AlCC1. The smallest size measured particles of dendritic were about ~ 50 nm which is at least twice smaller than those of AlCC1 in size, this indicate that the primary aluminium rich phase in aluminium- iron-silicon system of this work grew dendritically as predicted.

According to SEM with EDS scan in Fig. 7a–c it is observed that the characteristic feature of this morphology structure, the discrete Si particles dispersed in both boundary and interior of alpha aluminium matrix as clearly depicted from the closely amounts of Al and Si given in Fig. 7b, c. In contrast, Si distribution in conventional cast as seen in Fig. 5 usually spread with remarkable difference from point to point

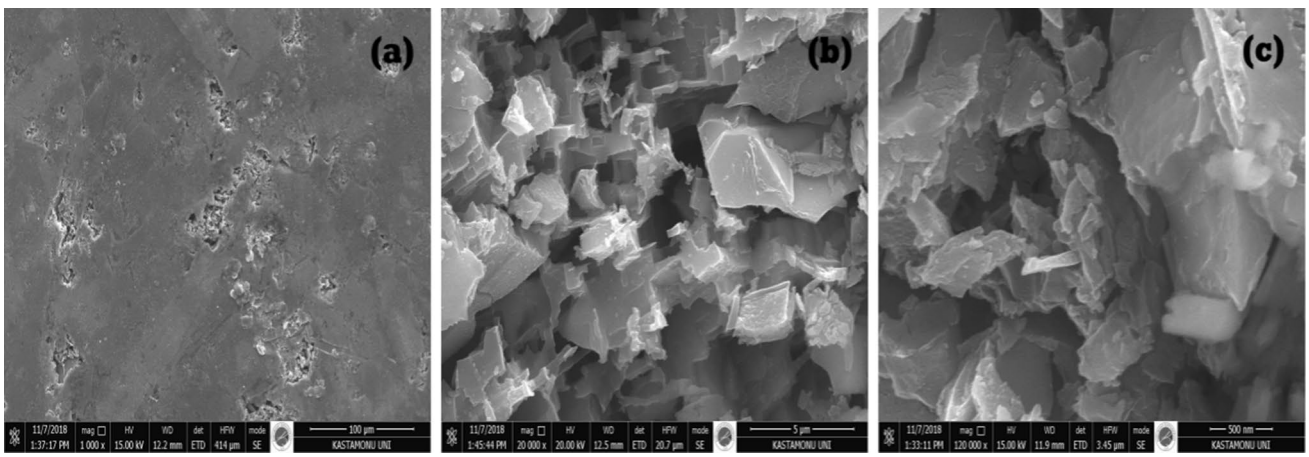

Fig. 4 The SEM images showing the microstructure of conventional cast AlCC1 at different magnifications **a** at 1000×, **b** at 20000×, **c** at 120000×

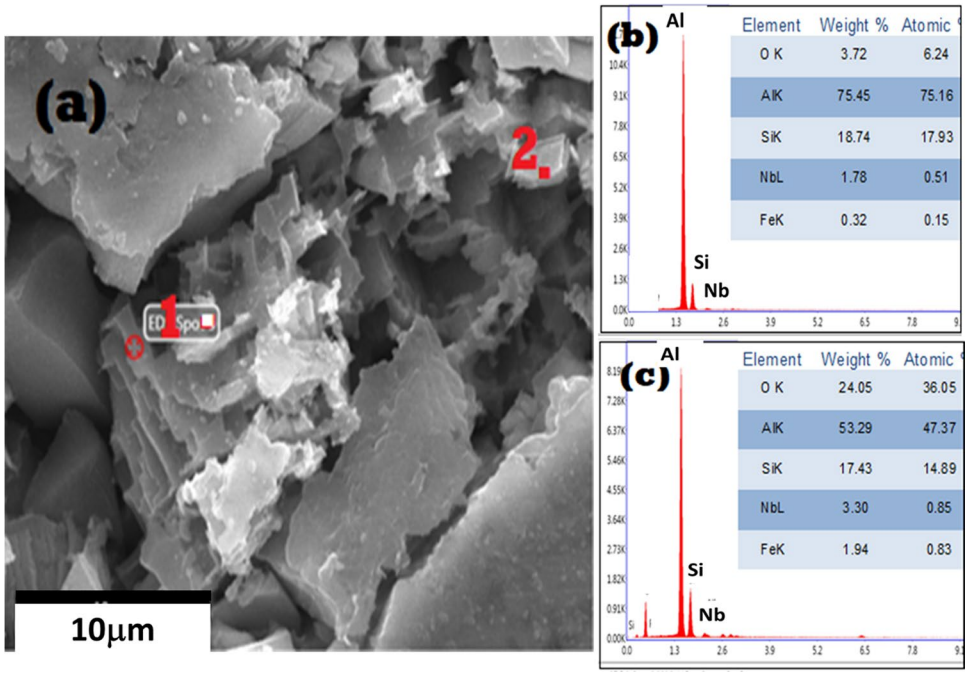

Fig. 5 SEM-EDS spectrum of detected particles for conventional cast AlCC1 **a**, **b** at point 1 and **c** at point 2

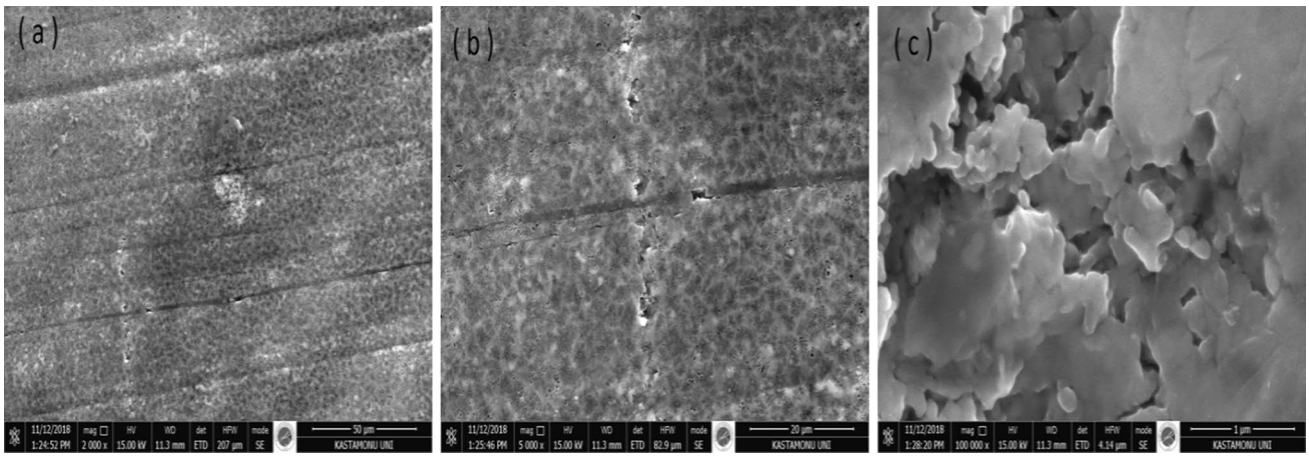

Fig. 6 The SEM images showing the microstructure of melt-spun AlMS1 at different magnifications **a** at 1000×, **b** at 20000×, **c** at 60000×

around α-Al matrix, indicated that rapid solidification has a significant effect on the solubility of elements through the phase constitution of Al–Si–Fe–Nb [31]. In other word, EDS analysis shows a remarkable difference in dispersion homogeneity of elements between a rapidly solidified ribbons and conventional cast which is not agree with [24], the general composition of elements within EDS scanned points 1 and 2, indicate that considerable amount of Si, Fe and Nb were dissolved into the intermetallic compound.

3.2.2 Microstructure of Conventional Cast AlCC2 and Melt-Spun AlMS2

Figure 3c, d show the optical micrographs of quinary alloys AlCC2 and AlMS2 respectively. Figure 3c illustrate the microstructure of conventional cast AlCC2 which is mainly comprising the following phases, (1) Si phase revealed as a different geometrical (light grey) forms with various dimensions within a range of (1–4 μm), (2) δ-Al_4(FeNiNb)Si_2 is

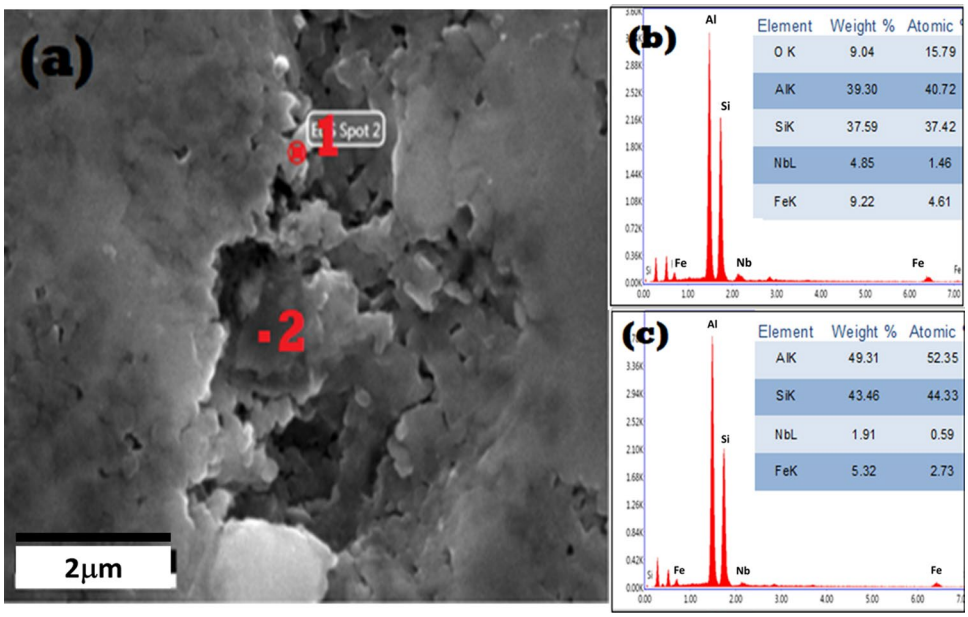

Fig. 7 SEM-EDS spectrum of detected particles for conventional cast AlMS1 **a**, **b** at point 1 and **c** at point 2

appeared as white chunks (coarse plate-lets) with different shapes and dimensions ≤ 10 µm. However, these coarse blocks are not well-defined boundary, diffuse with alpha-aluminium matrix through very tiny roots, (3) α-Al phase is the balance matrix in which even Si particles and tiny β-phase were contained. Figure 3d display the optic micrograph of a melt-spun AlMS2, despite the same constitution phases of melt-spun and conventional cast, it is difficult to recognize AlMS2 phases the microstructure is uniform and fine with dispersion of some crystals, as interpreted in case of AlMS1 Fig. 3b, because of high quench rate that exposed to, it appears to be feature less after etching [11, 29].

Figure 8a–c illustrate the microstructure of conventional cast AlCC2 in different degrees of magnification, Fig. 8a display the main phases of AlCC2 as pointed out and explained in Fig. 3c it is clear that the phases as seen in the image were interspersed with various discrete cavities which attributed to a trapped gases during solidification process. It can be noticed that from Fig. 8b, c the microstructure of AlCC2 reveal various sharp polygons and plates (represent Si phase and δ-phase, respectively) in the form of adjacent pyramids with different sizes, the average dimension of these geometrical forms as estimated from some corners were about 1 µm to 5 µm. It can be even seen from Fig. 8c some particles of different elements were scattered over the polygons with a size of ~ 100 nm.

Figure 9a–c show chemical composition of AlCC2 synthesized by EDS analysis at certain points, one can be clearly noticed that from Fig. 9b Ni and Nb distributions confirm their comprising in the intermetallic compounds which

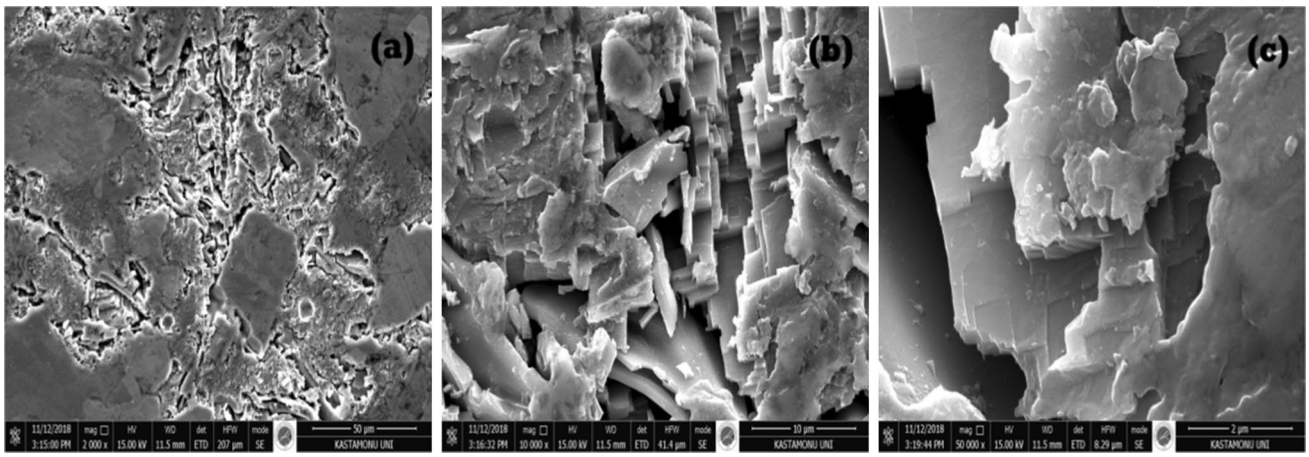

Fig. 8 The SEM images showing the microstructure of conventional cast AlCC2 at different magnifications **a** at 2000×, **b** at 10000×, **c** at 50000×

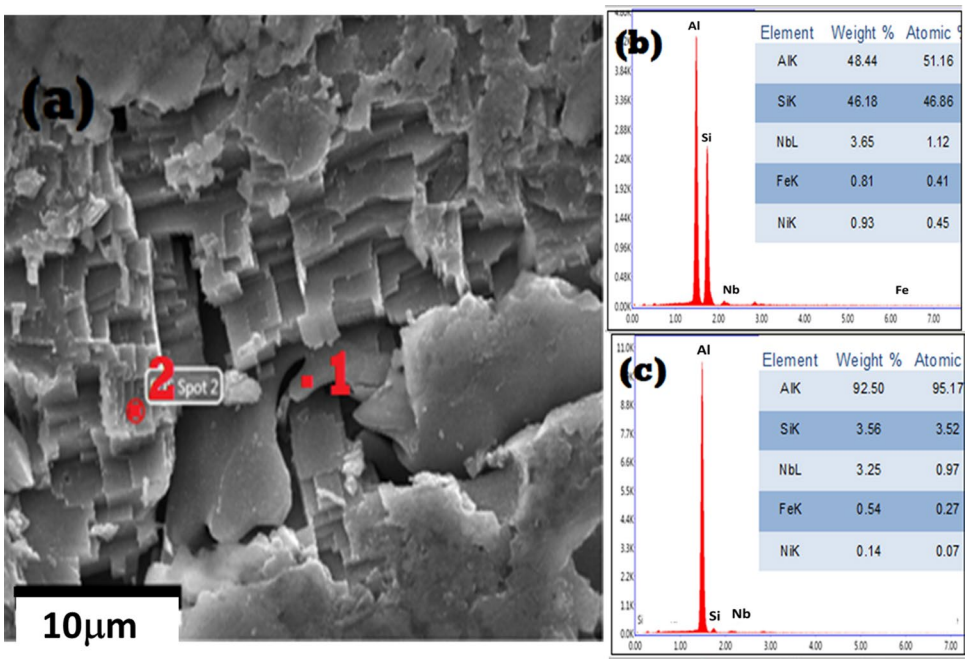

Fig. 9 SEM-EDS spectrum of detected particles for conventional cast AlCC2 **a**, **b** at point 1 and **c** at point 2

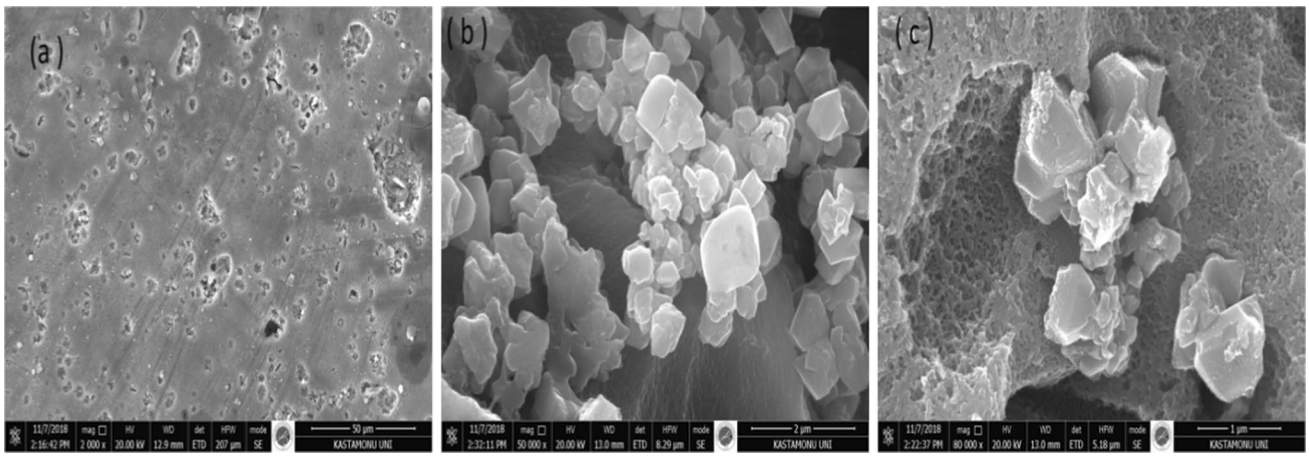

Fig. 10 The SEM images showing the microstructure of melt-spun AlMS2 at different magnifications **a** at 2000×, **b** at 50000×, **c** at 80000×

formed in both Al and Si phases. While Fig. 9c pointed out that intermetallic compounds formed in α-Al matrix according to the amounts of particles given in Fig. 9c.

Figure 10a–c show the morphology structure of melt-spun AlMS2. Figure 10a displays homogeneous and ultrafine structure comprising infinite scattered colonies with different diameters ranged from about 5 µm to 25 µm. From Fig. 10b, c the morphology of structure is dendritic, which has an average arm space of about. 100 ± 20 nm. Nano-crystalline particles scattered in these colonies with different quantities and dimensions, size range particles from 100 nm to 1 µm, these particles related to δ-Al_4(FeNiNb)Si_2 and primary Si Particles and it is difficult to distinguish them from each other. Therefore, it is known that such changes play an important role in improving mechanical properties [5, 29].

EDS analysis in Fig. 11a–c show that, Fe, NB and Ni intermetallic compounds formed in Si which distributed through a dendritic α-Al structure. In contrast to those of AlCC2 in Fig. 9, which shows low concentration of Si, Fe, Ni and Nb in some points on α-Al matrix, confirmed the low solubility of mentioned elements with conventional cast process . whereas the composition of scanned structure at point 1 and 2 as given in Fig. 11, indicate that the whole Si phase was dissolved into intermetallic compound according to the increasing of solid solubility resulted from using melt-spinning technique.

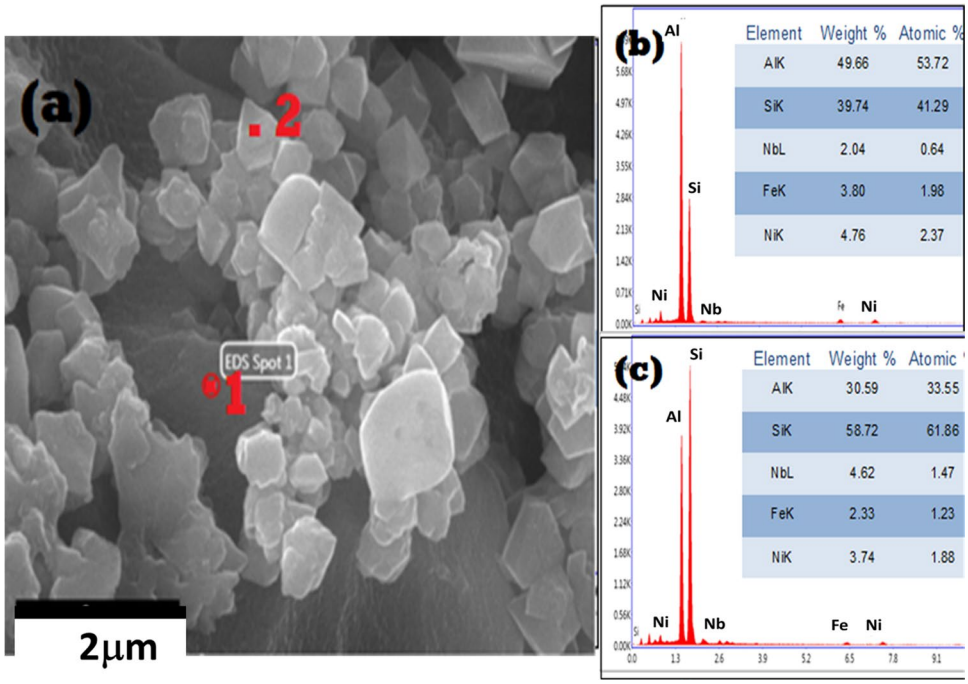

Fig. 11 SEM-EDS spectrum of detected particles for conventional cast AlMS2 **a**, **b** at point 1and **c** at point 2

4 Conclusion

In this paper, the Effect of Ni addition on morphology and microstructure of both conventional and melt-spun of Ai–Si–Fe–Nb (at wt%) alloy was investigated. Obtained results summarized that;

- Both intermetallic compounds δ–β phases coexisted in the as-cast Al–Si–Fe–Nb alloy.
- Only δ-phase existed in as-cast Al–Si–Fe–Nb–Ni alloy.
- XRD patterns of the ribbons of both Al–Si–Fe–Nb and Al–Si–Fe–Nb–Ni alloys, revealed only the peaks of α-Al phase.
- α-Al diffraction peaks of Al–Si–Fe–Nb ribbons, shifted to the relatively higher angles according to as-cast Al–Si–Fe–Nb alloy. In contrary, in the case of Al–Si–Fe–Nb–Ni ribbons shifted to the lower angles according to as-cast Al–Si–Fe–Nb–Ni alloy.
- Lattice parameter decreased from 0.4094 nm in as-cast Al–Si–Fe–Nb to 0.4067 nm in Al–Si–Fe–Nb ribbon, while in the case of Al–Si–Fe–Nb–Ni increased from 0.4075 nm in as-cast to 0.4094 nm in melt-spun.
- No evidence that Al–Si–Fe–Nb ribbons contains intermetallic copounds.
- Intermetallic compounds were ultra-fined and spheroid in Al–Si–Fe–Nb–Ni ribbons, evidenced that improvement of mechanical properties.

References

1. J. Yin, H. Cai, X. Cheng, H. Zhang, X. Zhang, Z. Xu, Enhanced mechanical properties due to nanocrystallization by isothermal annealing in Al85Ni9Er6 glassy alloy. J. Alloys Compd. **695**, e3048–e3053 (2017)
2. P. Rizzi, R. Doglione, L. Battezzati, Mechanical properties of Al-based amorphous/nanocrystalline alloys. Mater. Sci. Eng. A **375–377**, 969–974 (2004)
3. I. Lichioiu, I. Peter, B. Varga, M. Rosso, Preparation and structural characterization of rapidly solidified Al–Cu alloys. J. Mater. Sci. Technol. **30**(4), e394–e400 (2014)
4. M.K. Karaköse, Structural investigations of mechanical properties of Al based rapidly solidified alloys. Mater. Des. **32**, 4970–4979 (2011)
5. E. Karaköse, T. Karaaslan, O. Uzun, M. Keskin, Microstructure evolution and microhardness of a melt-spun Al–6Ni–2Cu–1Si (in wt%) alloy. J. Mater. Process. Technol. **195**, 58–62 (2008)
6. M.F. Kilicaslan, E. Karaköse, Production of CNT-bearing melt-spun Al–2Sc–0.05CNT alloys. J. Alloys Compd. **738**, e182–e187 (2018)
7. L. Katgerman, F. Domb, Rapidly solidified aluminium alloys by meltspinning. Mater. Sci. Eng. A **375–377**, 1212–1216 (2004)
8. Y. Lin, S. Mao, Z. Yan, Y. Zhang, L. Wang, The enhanced microhardness in a rapidly solidified Al alloy. Mater. Sci. Eng. A **692**, 182–191 (2017)
9. Z. Zhang, X. Bian, Y. Wang, Effect of temperature and wheel speed on the microstructure of melt-spun Al–20Cu alloy. J. Alloy. Compd. **349**, 185–192 (2003)
10. R.C. Budhani, T.C. Goel, K.L. Chopra, Melt-spinning technique for preparation of metallic glasses. Bull. Mater. Sci. **4**(5), 549–561 (1982)

11. N. Ülü, A. Genç, M. Öveçoğlu, N. Eruslua, F. Froes, Characterization investigations of melt-spun ternary Al–xSi–3.3Fe (x = 10, 20 wt%) alloys. J. Alloys Compd. **322**, 249–256 (2001)
12. S. Chen, J. Chen, S. Lin, Y. Lin, Effects of B upon glass forming ability of Al87Y8Ni5 amorphous alloy. J. Alloys Compd. **565**, 29–36 (2013)
13. D.H. Kim, W.T. Kim, Formation and crystallization of Al–Ni–Ti amorphous alloys. Mater. Sci. Eng. A **385**, 44–53 (2004)
14. M. Rajabi, A. Simchia, P. Davamia, Microstructure and mechanical properties of Al–20Si–5Fe–2X (X = Cu, Ni, Cr) alloys Produced by melt-spinning. Mater. Sci. Eng. A **492**, 443–449 (2008)
15. M. Andrzejczuk, M. Lewandowska, J. Latuch, K. Jan, Multiscale characterization of nanostructured Al–Si–Zr alloys obtained by rapid solidification method. J. Mater. Sci. **46**, 5454–5459 (2011)
16. Y. Lin, B. Wu, S. Li, S. Mao, X. Liu, Y. Zhang, L. Wang, The quantitative relationship between microstructure and mechanical property of a melt-spun Al–Mg alloy. Mater. Sci. Eng. A **621**, 212–217 (2015)
17. P. Squire, I. Change, Development of rapidly solidified Al–Y–Ni based alloys. Mater. Sci. Eng. A **449–451**, 1009–1012 (2007)
18. W. Zhang, S. Chen, Z. Zhu, H. Wang, Y. Li, H. Kato, H. Zhang, Effect of substituting elements on thermal stability and glass forming ability of an Al–Ni–Er metallic glass. J. Alloy. Compd. **707**, 97–101 (2017)
19. T. Nagase, M. Takemura, M. Matsumuro, M. Matsumoto, Y. Fujii, Design and microstructure analysis of globules in Al–Co–La–Pb immiscible alloys with an amorphous phase. Mater. Des. **117**, 338–345 (2017)
20. C. Chena, W. Hsub, S. Chenb, Role of Sc on the glass forming ability and mechanical properties of Al–Y–Ni–Sc bulk metallic glass produced with different cooling rates. Mater. Sci. Eng. A **725**, 119–126 (2018)
21. A. Aronin, D. Matveev, E. Pershina, V. Tkatch, The effect of changes of Al-based amorphous phase structure on structure forming upon crystalline. J. Alloys Compd. **715**, e176–e183 (2017)
22. M. Kiliçaslan, F. Yilmazb, S. Ergneb, S. Hongc, O. Uzund, Microstructure and microhardness of melt-spun Al–25Si–5Fe–xCo (x = 0, 1, 3, 5) alloys. Mater. Charact. **77**, 15–22 (2013)
23. F. Prusa, M. Blahova, V. Kucera, A. Mechalcova, High-strength ultra-fine-grained hypereutectic Al–Si–Fe–X (X = Cr, Mn) alloys prepared by short-term mechanical alloying and spark plasma sintering. Materials (Basel) **9**(12), 973 (2016). https://doi.org/10.3390/ma9120973
24. E. Karaköseа, M. Keskinb, Microstructures and microhardness evolutions of melt-spun Al–8Ni–5Nd–4Si alloy. Mater. Charact. **65**, 37–47 (2012)
25. M. Shafizadih, H. Aashuri, K. Ferasat, S. Nikzad, Microstructural modification of Al–30Si–5Fe alloy using a combination of rapid solidified and thixoforming processes. Metallogr. Microstruct. Anal. **5**, 217–228 (2016)
26. K. H. Harbbi, S. S. Jahil. Study the lattice distortion and particle size of one phase of MnO by using fourier analysis of X-ray diffraction lines. Adv. Phys. Theor. Appl. **65** (2017). ISSN 2225-0638 (Online)
27. T.H. Lee, S.J. Hong, Microstructure and mechanical properties of Al–Si–X alloys fabricated by gas atomization and extrusion process. J. Alloys Compd. **487**, 218–224 (2009)
28. M. Rajabia, M. Vahidia, A. Simchia, P. Davamia, Effect of rapid solidification on the microstructure and mechanical properties of hot-pressed Al–20Si–5Fe alloys. Metals Charact. **60**, 1370–1381 (2009)
29. E. Karaköse, M. Keskinb, Morphological characteristic of the conventional and melt-spun Al–10Ni–5.6Cu (in wt%) alloy. Mater. Charact. **60**, 1569–1577 (2009)
30. X. Dong, L. He, G. Mi, P. Li, Two directional microstructure and effects of nanoscale dispersed Si particles on microhardness and tensile properties of AlSi7Mg melt-spun alloy. J. Alloys Compd. **618**, 609–614 (2015)
31. Y. Wang, Z. Zhang, S. Zheng, X. Bian, TEM observations of a rapidly solidified Al–20Sb alloy. J. Alloys Compd. **370**, 159–163 (2004)